A S_N2 Reaction That Avoids Its Deep Potential Energy Minimum

Lipeng Sun,[1] Kihyung Song,[2] William L. Hase[1]*

Chemical dynamics trajectory simulations were used to study the atomic-level mechanisms of the $OH^- + CH_3F \rightarrow CH_3OH + F^-$ S_N2 nucleophilic substitution reaction. The reaction dynamics, from the $[OH\cdot\cdot CH_3\cdot\cdot F]^-$ central barrier to the reaction products, are simulated by ab initio direct dynamics. The reaction's potential energy surface has a deep minimum in the product exit channel arising from the $CH_3OH\cdot\cdot F^-$ hydrogen-bonded complex. Statistical theories of unimolecular reaction rates assume that the reactive system becomes trapped in this minimum and forms an intermediate, with random redistribution of its vibrational energy, but the majority of the trajectories (90%) avoided this potential energy minimum and instead dissociated directly to products. This finding is discussed in terms of intramolecular vibrational energy redistribution (IVR) and the relation between IVR and molecular structure. The finding of this study may be applicable to other reactive systems where there is a hierarchy of time scales for intramolecular motions and thus inefficient IVR.

Many chemical reactions have a potential energy surface (PES) with one or more "wells," which are potential energy minima on the reaction path connecting reactants and products (*1*). Furthermore, the PES may have additional wells that are not on the path but are accessible via pathways with potential energy barriers smaller than those required to form products or return to reactants. These types of reactions include enzyme catalysis (*2*), isomerizations of organic molecules (*3*), and S_N2 nucleophilic substitution (*4*, *5*). The standard paradigm for their chemical kinetics and dynamics is that as the atoms undergo their cooperative "dance" in progressing from reactants to products, they "find" these wells, becoming trapped in each for a period of time, forming reaction intermediates (*6*). Furthermore, rapid intramolecular vibrational energy redistribution (IVR) (*7*) is often assumed to occur and give rise to a statistical intermediate in which energy is randomized between its vibrational modes. Given these assumptions, the actual dynamics of the PES are not needed to interpret the reaction's kinetics. As embodied in Rice-Ramsperger-Kassel-Marcus theory (*1*) and its extensions (*8*), and in combination with transition state (TS) theory (*9*), the only information required to calculate the reaction rate and intermediate lifetimes is the properties of the reactants and potential energy wells and of TSs, which connect the reactants, wells, and products.

The above assumptions transform the actual reaction dynamics into a purely statistical model (*1*, *6*). Nonetheless, nonstatistical dynamics are often very important (*4*, *6*, *10*). Recent advances in spectroscopic (*11*, *12*), theoretical, and computational methods now allow the dynamics of a many-atom reactive system to be probed as it moves on its PES. Electronic structure theory and molecular dynamics can now be coupled directly, so that trajectories may be calculated on the fly without the need for an analytic PES (*13*, *14*). This general methodology extends trajectory simulations to a broad range of chemical systems (*14*).

The study of gas-phase S_N2 nucleophilic substitution reactions explores the limit of the statistical model for chemical reactions (*4*, *5*). From both experiments (*5*) and classical trajectory (*4*, *6*) and quantum dynamical simulations (*15*, *16*), extensive nonstatistical dynamics have been observed for S_N2 reactions of the type

$$X^- + CH_3Y \rightarrow XCH_3 + Y^- \tag{1}$$

where X^- and Y^- are halide ions. Included among the nonstatistical dynamics are a direct reaction pathway without trapping in either the $X^-\cdot\cdot\cdot CH_3Y$ or $XCH_3\cdot\cdot\cdot Y^-$ potential energy well (*17*), mode-specific decomposition of the $X^-\cdot\cdot\cdot CH_3Y$ and $XCH_3\cdot\cdot\cdot Y^-$ complexes with inefficient IVR (*15*, *18*), extensive recrossing of the $[X\cdot\cdot\cdot CH_3\cdot\cdot\cdot Y]^-$ central barrier region of the PES (*14*, *19*), nonstatistical energy distributions for the reaction products (*4*, *20*), and a dependence of the reaction rate on translational, rotational, and vibrational energies inconsistent with the statistical model (*21–25*). In contrast to the richness of the nonstatistical dynamics for reaction 1, the statistical model gives a rate constant for the $Cl^- + ClCH_2CN \rightarrow ClCH_2CN + Cl^-$ S_N2 reaction that is in excellent agreement with the experimental value (*26*). However, for proton transfer between methanol and methoxide and in homologous systems ($ROH + R'O^-$, where R and R are alkyl groups), which is similar to reaction 1, a statistical model is insufficient for explaining the kinetics (*10*).

A further understanding of the dynamics of gas-phase S_N2 reactions can be had by examining reactions in which one of the halide ions is a strong base, such as OH^-. Experiments that probed the kinetics of

$$OH^- + CH_3F \rightarrow CH_3OH + F^- \tag{2}$$

did not reveal any information concerning the dynamics of possible reaction intermediates (*27*). Ab initio electronic structure calculations for this reaction show a PES with a double well (*28–30*). However, instead of having a post-reaction potential energy well with the traditional S_N2 structure of the halide ion bound to the back side of the CH_3 moiety, there is a global minimum with the halide bound to CH_3OH via a hydrogen bond; that is, $CH_3OH\cdot\cdot F^-$, with a deep well with respect to the $CH_3OH + F^-$ reaction products.

In the study reported here, a direct dynamics classical trajectory simulation is used to study the dynamics of reaction 2 as it moves from the $[HO\cdot\cdot CH_3\cdot\cdot F]^-$ central barrier to the $CH_3OH + F^-$ products. The simulations illustrate how PES properties control the degree of nonstatistical behavior and IVR in chemical reactions with potential energy wells, and that the atomic-level mechanism of a chemical reaction cannot be ascertained from a visual inspection of its PES. For the system studied here, the fundamental interest is how the deep $CH_3OH\cdot\cdot F^-$ potential energy well affects the reaction dynamics. The first step in the study is to establish the level of ab initio theory that is both accurate and practical for the simulations.

The $OH^- + CH_3F \rightarrow CH_3OH + F^-$ PES. The CCSD(T) and MP2 ab initio theories (*31*) are used to characterize the PES for reaction 2. There are three stationary points between the reactants and products: (i) the $OH^-\cdot\cdot CH_3F$ S_N2-like potential energy well; (ii) the $[HO\cdot\cdot CH_3\cdot\cdot F]^-$ central barrier; and (iii) the $CH_3OH\cdot\cdot F^-$ potential energy well, with a hydrogen bond between OH and F^-. For this reaction, there is not a traditional energy minimum with F^- attached to the back side of CH_3OH. The structures of these stationary points, determined with the MP2 electronic structure theory and 6-31+G* and 6-311++G(2df,2pd) basis sets, are shown in Fig. 1. Overall, the 6-31+G* and 6-311++G(2df,2pd) geometries are in very good agreement. Their largest differences are for the C-F bond length, the H-O··C angle at the central barrier, and the O-H and H··F bond lengths for the $CH_3OH\cdot\cdot F^-$ minimum. The latter bond lengths are shorter by 0.03 Å

---

[1] Department of Chemistry, Wayne State University, Detroit, MI 48202, USA. [2] Department of Chemistry, Korea National University of Education, Chongwon, Chungbuk 363–791 Korea.

*To whom correspondence should be addressed. E-mail: wlh@cs.wayne.edu

and longer by 0.135 Å, respectively, with the smaller 6-31+G* basis set.

The MP2 and CCSD(T) energies for the stationary points on the PESs are listed in Table 1. The large difference between the MP2 energies with the 6-31G* and 6-31+G* basis sets illustrates the importance of diffuse functions to obtain accurate energies for this S_N2 reaction. The CCSD(T) and MP2 energies for the largest basis sets—6-311++G(2df,2pd) and aug-cc-pVTZ—are in good agreement and predict a central barrier with an energy ~3 kcal/mol less than that of the reactants, a reaction exothermicity of ~20 kcal/mol, and a $CH_3OH\cdot\cdot F^-$ potential energy minimum ~30 kcal/mol below the product asymptotic limit. The latter well depth is in excellent agreement with the 298 K F^- + CH_3OH association enthalpy of 30 ± 1 kcal/mol (*32*). Experimental energies are not available for the other stationary points.

From an analysis of the computer times required to calculate a direct dynamics trajectory at the different levels of theory and the accuracy of these different theories, MP2/6-31+G* theory was chosen for the trajectory simulation study. This level of theory gives relative energies for the $[HO\cdot\cdot\cdot CH_3\cdot\cdot\cdot F]^-$, $CH_3OH\cdot\cdot F^-$, and CH_3OH + F^- stationary points within 3 kcal/mol of the values obtained with the highest levels of theory.

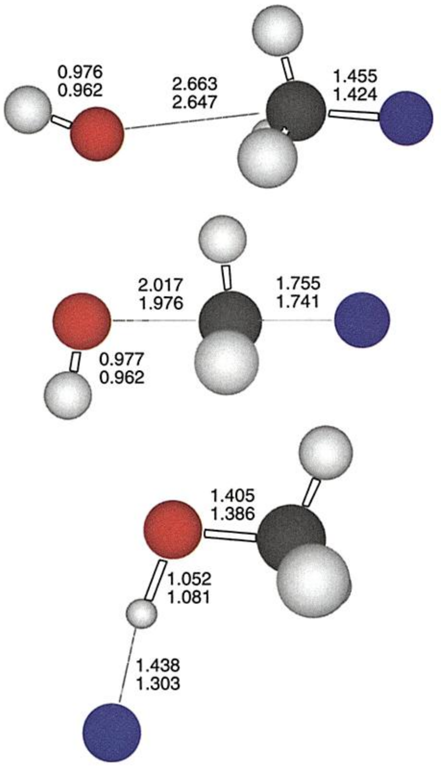

Fig. 1. MP2/6-31+G* and 6-311++G(2df,2pd) geometries for the $HO^-\cdot\cdot\cdot CH_3F$ well, $[HO\cdot\cdot CH_3\cdot\cdot F]^-$ barrier, and $CH_3OH\cdot\cdot\cdot F^-$ well. The lower set of bond distances, in angstroms, are for the 6-31+G* basis set. The respective 6-31+G* and 6-311++G(2df,2pd) values for the angles are as follows: $HO^-\cdot\cdot\cdot CH_3F$ well: H-O···C, 153.3 and 171.9°; and O···C-F, 169.0 and 135.4°. $[HO\cdot\cdot CH_3\cdot\cdot F]^-$ barrier: H-O···C, 108.8 and 104.0°; and O···C···F, 177.1 and 177.9°. $CH_3OH\cdot\cdot\cdot F^-$ well: $F^-\cdot\cdot\cdot$H-O, 174.0 and 176.6°; and H-O-C, 106.3 and 106.2°. The H-O···C-F, H-O··C-H, and H-O-C-H dihedral angles are 180° for the three respective stationary points.

The complete intrinsic reaction coordinate (IRC) (*33*) connecting the reactants and products was calculated with the MP2/6-31+G* theory by initializing the IRC calculations at the central barrier and near the reactant and product asymptotic limits. Energies and geometries along the IRC are shown in Fig. 2. The initial IRC, from the central barrier toward products, involves F^- dissociation along an approximate O-C-F collinear axis. At *s* of about 5 atomic mass units ($amu^{1/2}$)–Bohr, the IRC enters a flat region that is apparently a remnant of a back-side potential energy minimum that is "lost" because of the presence of the much deeper $CH_3OH\cdot\cdot F^-$ hydrogen-bonded minimum. At *s* of approximately 12 $amu^{1/2}$-Bohr, the IRC leaves the flat region and starts its descent into the $CH_3OH\cdot\cdot F^-$ minimum.

Reaction dynamics. Ab initio direct dynamics trajectory calculations, performed with the VENUS96 (*34*) and GAUSSIAN98 program packages (*31*), were used to simulate the reaction dynamics. The MP2/6-31+G* theory was used for the calculations because it correctly represents the PES obtained at a much higher level of theory and is a practical approach for performing direct dynamics simulations. The relative computer processing time to integrate trajectories with the MP2 theory and the 6-31+G*, 6-31++G**, 6-311++G**, and 6-311++G(2df,2pd) basis sets was 1.00, 2.39, 4.09, and 92.37, respectively.

The direct dynamics trajectories were initiated at the central barrier, with conditions chosen from a 300 K Boltzmann distribution for reaction coordinate translation, the 14 vibrational degrees of freedom, and the three external rotations (*34*, *35*). Quasiclassical sampling (*35*), which includes zero-point energy, was used to choose initial conditions for the trajectories. The trajectories were integrated with a Hessian-based predictor-corrector algorithm (*36*), which includes updating of the Hessian matrix (*37*). The trajectory was terminated after 3 ps of motion or when the F^- and CH_3OH product separation exceeded 17 Å. The relative energy and angular

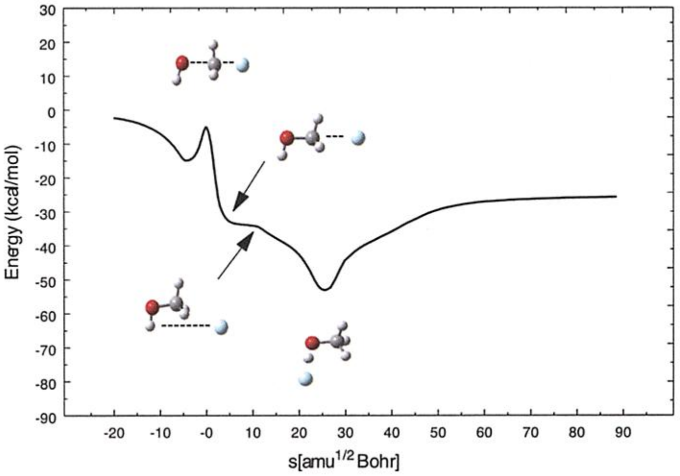

Fig. 2. Potential energy along the IRC for OH^- + $CH_3F \rightarrow CH_3OH$ + F^-. *s* is the distance along the IRC.

Table 1. Electronic structure theory energies (in kcal/mol) for OH^- + $CH_3F \rightarrow CH_3OH$ + F^- stationary points with respect to the OH^- + CH_3F reactants. Zero-point energies are not included. The basis set is 6-311++G(2df,2pd) for the lower MP2 calculations. The basis sets for the three CCSD(T) calculations are 6-311++G(2df,2pd), aug-cc-pVTZ, and TZ2pf + dif, respectively. For CCSD(T) (*3*), the calculations are from (*30*).

Theory	Stationary points			
	$OH^-\cdot\cdot\cdot CH_3F$	$[HO\cdot\cdot\cdot CH_3\cdot\cdot\cdot F]^-$	$CH_3OH\cdot\cdot\cdot F^-$	F^- + CH_3OH
MP2/6-31G*	−23.55	−12.30	−68.19	−14.90
MP2/6-31+G*	−14.89	−5.05	−53.55	−24.99
MP2/6-31++G**	−15.10	−4.62	−52.80	−23.67
MP2/6-311++G**	−14.21	−1.32	−52.50	−22.78
MP2	−14.10	−2.99	−52.21	−19.94
CCSD(T) (1)	−14.36	−3.91	−52.43	−19.84
CCSD(T) (2)	−13.91	−3.02	−49.95	−19.59
CCSD(T) (3)	−13.78	−3.05	−50.88	−20.80

momentum were conserved to within 0.01 kcal/mol and $10^{-8}\,\hbar$, respectively (where $\hbar$ is Planck's constant divided by 2π). The actual computer processing time for a trajectory ranged from 2 to 6 days on a two-processor Pentium III 733-MHz workstation.

Sixty-four trajectories were initiated at the $[OH\cdot\cdot CH_3\cdot\cdot F]^-$ central barrier, with the sign of the reaction coordinate momentum chosen randomly; that is, directed toward either reactants or products. Of these trajectories, 33 formed a reaction intermediate in the $HO^-\cdot\cdot CH_3F$ pre-reaction potential energy well. Two reaction pathways were identified for the remaining 31 trajectories. One followed the IRC, and the system became trapped in the deep $CH_3OH\cdot\cdot F^-$ potential energy well and formed a reaction intermediate. Four of the trajectories were of this type, of which one formed the $CH_3OH + F^-$ reaction products during the 3 ps of the trajectory integration. The remaining 27 trajectories followed the second pathway, which was a direct dissociation, with departure of the F^- ion approximately along the O-C$\cdot\cdot$F$^-$ collinear axis. These two pathways are depicted in Fig. 3 for two of the trajectories calculated in this study. Only a small fraction (~10 %) of the trajectories actually followed the IRC reaction path. The vast majority of the trajectories followed a non-IRC direct dissociation path, for which ~1 ps was required for the system to move from the central barrier to the F^- and CH_3OH products separated by 17 Å. Recrossing of the central barrier is unimportant for this reactive system. Of the 64 trajectories, there was a nonstatistical single barrier recrossing for only 4, and no trajectories underwent multiple recrossings. The unimportance of barrier recrossing for $OH^- + CH_3F \rightarrow CH_3OH + F^-$ is in sharp contrast to what was observed for $Cl^- + CH_3Cl \rightarrow ClCH_3 + Cl^-$ and $Cl^- + CH_3Br \rightarrow ClCH_3 + Br^-$ (*12*, *16*, *17*). Identifying the origin of this difference will require further work. The origin of the propensity for the direct reaction path is seen in the PES diagram in Fig. 4, in which potential energy is plotted versus the C$\cdot\cdot$F$^-$ distance and the O-C$\cdot\cdot$F$^-$ angle. The release of potential energy to the asymmetric O-C$\cdot\cdot$F$^-$ stretch motion of the reaction coordinate, as the system moves off the central barrier, tends to propel F^- from CH_3OH, with the O-C$\cdot\cdot$F$^-$ angle maintained at nearly 180°. The PES is rather flat for bending of the O-C$\cdot\cdot$F$^-$ angle, and there is only a very weak force to pull the reactive system from the direct dissociation reaction path into the $CH_3OH\cdot\cdot F^-$ potential energy well with a C-O$\cdot\cdot$F$^-$ angle of 102.8°. In the language of IVR, there is very weak coupling between $CH_3OH + F^-$ relative translation and O-C$\cdot\cdot$F$^-$ bending and other vibrational degrees of freedom of the reactive system. As the system moves off the central barrier, it moves directly to products without forming an intermediate trapped in the $CH_3OH\cdot\cdot F^-$ potential energy well.

The nature of the energy distribution of the reaction products is often used to probe the atomic-level mechanisms of chemical reactions with potential energy wells. This analysis is most useful if there is not a poten-

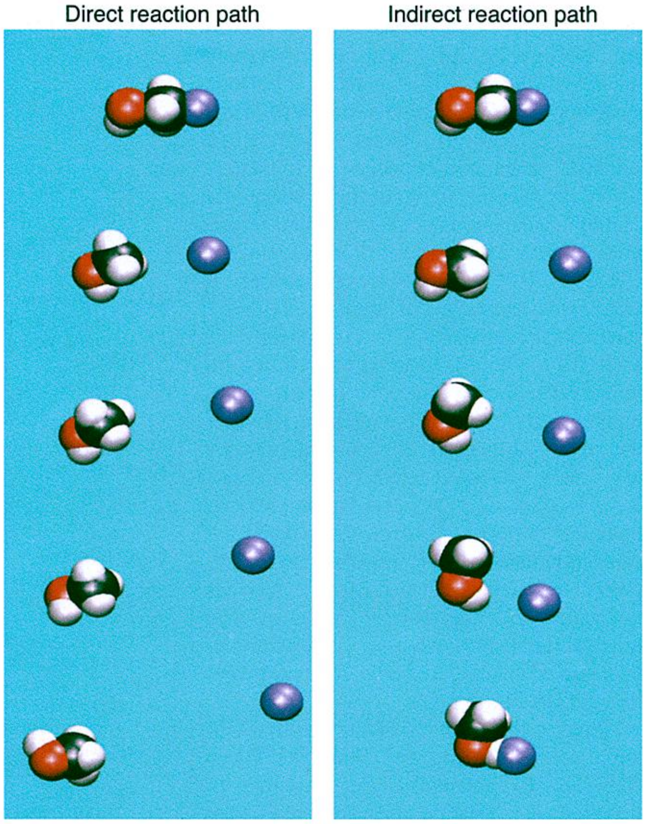

Fig. 3. The two pathways for motion from the $[HO\cdot\cdot CH_3\cdot\cdot F]^-$ central barrier to the $CH_3OH + F^-$ reaction products. Most of the trajectories follow the direct dissociation path. A small amount, ~10%, form the $CH_3OH\cdot\cdot F^-$ hydrogen-bonded intermediate and follow an indirect path.

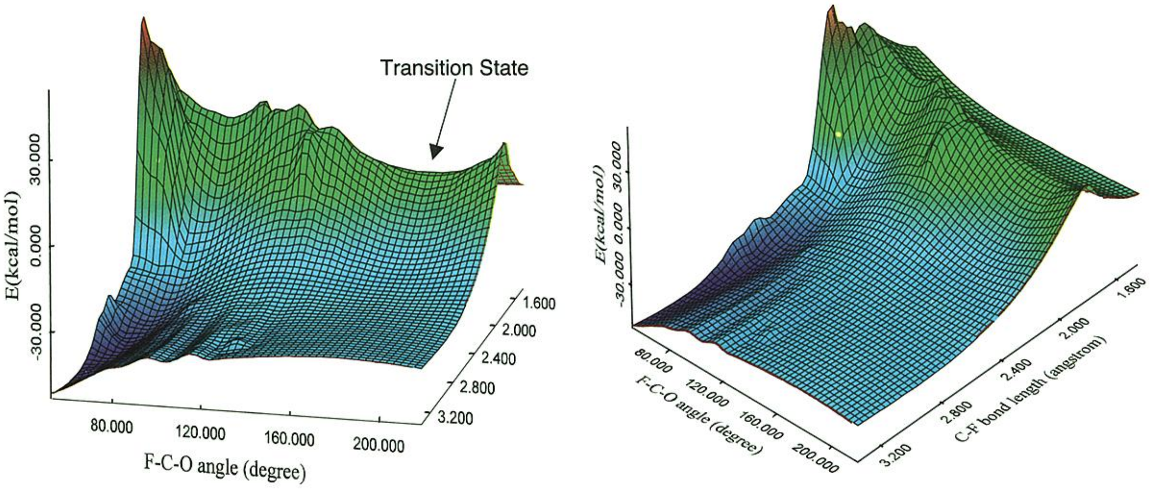

Fig. 4. Potential energy contour diagram for $[HO\cdot\cdot CH_3\cdot\cdot F]^-$ fragmentation as a function of the C-F distance and the O-C$\cdot\cdot$F angle. The remaining coordinates are optimized at each point on the PES.

tial energy barrier for association of the reaction products; that is, no exit channel potential energy release as the products separate (*38*). If the product energies for such reactive systems are distributed statistically over the available energy states, it is often assumed that the reaction proceeds through a statistical reaction intermediate, with its energy randomized among its vibrational degrees of freedom (*1*). However, this correspondence is not definitive, because a statistical product energy distribution may be observed for a nonstatistical reaction intermediate (*39*). Nevertheless, it is of interest to consider the energy distribution of the $F^- + CH_3OH$ reaction products, because there is no barrier to their association and movement into the $CH_3OH\cdots F^-$ potential energy well.

The available product energy is distributed between relative translation of the $F^- + CH_3OH$ products E_t, CH_3OH rotation E_r, and CH_3OH vibration E_v. The trajectory distributions for these product energies are given in Fig. 5, where they are compared with the prediction of phase space theory (PST) (*40*), which assumes that the available energy is distributed statistically between the product energy states. The trajectory average energies are $\langle E_t \rangle = 3.9$, $\langle E_r \rangle = 1.1$, and $\langle E_v \rangle = 17.9$ kcal/mol, with the CH_3OH harmonic zero point energy removed from E_v. In comparison, the PST values for these respective energies are 3.1, 4.2, and 15.5 kcal/mol. Though the PST and trajectory distributions are not the same, their differences are rather small and not as large as observed for other S_N2 reactions (*4*, *20*). It may be possible to measure the product energy distributions, particularly the one for translation (*14*), and compare them with the trajectory distributions. Differences between the experimental and PST product energy distributions would be consistent with a direct reaction mechanism, without trapping in the $CH_3OH\cdots F^-$ potential energy well, as predicted by the trajectory simulations.

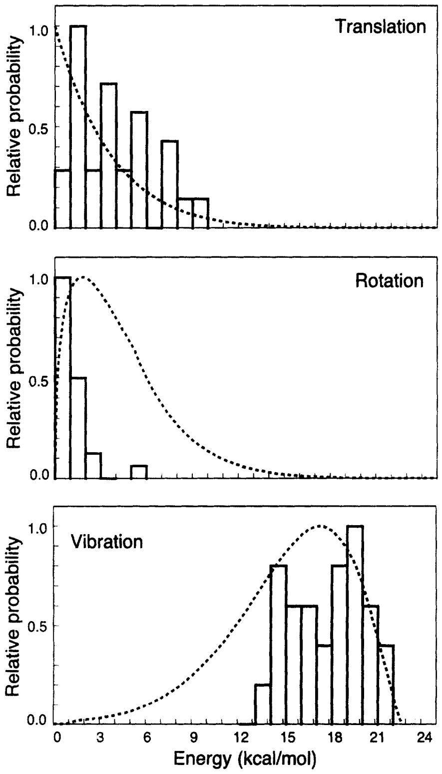

Fig. 5. Translation, rotation, and vibration energy distributions of the reaction products. The dashed line is the statistical (PST) prediction, and the histogram is the trajectory result.

Dynamics, time scales, and PESs. The computer simulations reported here illustrate that the evaluation of PES features such as well depths, barrier heights, and intrinsic reaction coordinates is insufficient for determining atomic-level mechanisms for chemical reactions. Instead, it is necessary to study the actual motion of the atoms on a reactive system's PES. The simulations also show how the efficiency of IVR and formation of a statistical reaction intermediate are intimately linked to the hierarchy of time scales for intramolecular motions and structural transitions on the PES. Inefficient formation of the $CH_3OH\cdots F^-$ reaction intermediate arises from rapid separation of the $CH_3OH + F^-$ products in comparison to the longer time scale for $C\text{-}O\cdots F^-$ bending to form the intermediate. Such a hierarchy of time scales has been observed in previous work, where the structural changes of a solvent cage are too slow to allow a reactive system to access its deep potential energy minimum (*41*). A hierarchy of time scales and inefficient access of deep potential energy minima may be important in enzyme catalysis, where motions associated with the reaction center may be much faster than those associated with conformational changes and other multiatom motions of the enzyme (*2*).

Finally, the inability of the reactive system studied here to find the deep $CH_3OH\cdots F^-$ potential energy minimum illustrates the relation between inefficient structural transitions and inefficient IVR. This relation has also been identified in the unimolecular decomposition of fluxional molecules, for which fast transitions between multiple potential energy wells are required for statistical behavior (*42*). At a quite fundamental level, energy transfer between vibrational modes involves structural changes, for when energy flows between bonds, one bond lengthens and the other shortens. The simulations reported here illustrate the intimate relationship between IVR and structure (*43*).

References and Notes

1. T. Baer, W. L. Hase, *Unimolecular Reaction Dynamics. Experiments and Theory* (Oxford Univ. Press, New York, 1996).
2. A. Fersht, *Enzyme Structure and Mechanism* (Freeman, New York, ed. 2, 1985).
3. J. E. Baldwin, in *The Chemistry of the Cyclopropyl Group*, vol. 2, Z. Rappoport, Ed. (Wiley, London, 1995), pp. 469–493.
4. W. L. Hase, *Science* **266**, 998 (1994).
5. M. L. Chabinyc, S. L. Craig, C. K. Regan, J. I. Brauman, *Science* **279**, 1882 (1998).
6. W. L. Hase, *Acc. Chem. Res.* **31**, 659 (1998).
7. T. Uzer, *Phys. Rep.* **199**, 73 (1991).
8. M. Quack, J. Troe, *Ber. Bunsenges. Phys. Chem.* **78**, 240 (1974).
9. J. I. Steinfeld, J. S. Francisco, W. L. Hase, *Chemical Kinetics and Dynamics* (Prentice-Hall, Upper Saddle River, NJ, ed. 2, 1999).
10. K. F. Lim, J. I. Brauman, *J. Chem. Phys.* **94**, 7164 (1991).
11. A. H. Zewail, *Science* **242**, 1645 (1988).
12. R. B. Metz, A. Weaver, S. E. Bradforth, T.-N. Kitsopoulos, D. M. Neumark, *J. Phys. Chem.* **94**, 1377 (1990).
13. R. Car, M. Parrinello, *Phys. Rev. Lett.* **55**, 2471 (1985).
14. K. Bolton, W. L. Hase, G. H. Peslherbe, in *Multidimentional Molecular Dynamics Methods*, D. L. Thompson, Ed. (World Scientific, London, 1998), pp. 143–189.
15. M. I. Hernández, J. Campos-Martinez, P. Villarreal, S. Schmatz, D. C. Clary, *Phys. Chem. Chem. Phys.* **1**, 1197 (1999).
16. S. Schmatz, P. Botschwina, J. Hauschildt, R. Schinke, *J. Chem. Phys.* **114**, 5233 (2001).
17. S. R. Vande Linde, W. L. Hase, *J. Chem. Phys.* **93**, 7962 (1990).
18. D. S. Tonner, T. B. McMahon, *J. Am. Chem. Soc.* **122**, 8783 (2000).
19. L. Sun, W. L. Hase, K. Song, *J. Am. Chem. Soc.* **123**, 5753 (2001).
20. S. T. Graul, M. T. Bowers, *J. Am. Chem. Soc.* **116**, 3875 (1994).
21. A. A. Viggiano, R. A. Morris, J. S. Paschkewitz, J. F. Paulson, *J. Am. Chem. Soc.* **114**, 10477 (1992).
22. H. Wang, W. L. Hase, *J. Am. Chem. Soc.* **117**, 9347 (1995).
23. S. L. Craig, J. I. Brauman, *J. Phys. Chem. A* **101**, 4745 (1997).
24. V. F. DeTuri, P. A. Hintz, K. M. Ervin, *J. Phys. Chem. A* **101**, 5969 (1997).
25. S. Kato, G. E. Davico, H. S. Lee, C. H. DePuy, V. M. Bierbaum, *Int. J. Mass Spectrom.* **210**, 223 (2001).
26. A. A. Viggiano *et al.*, *J. Am. Chem. Soc.* **116**, 2213 (1994).
27. C. H. DePuy, S. Gronert, A. Mullin, V. M. Bierbaum, *J. Am. Chem. Soc.* **112**, 8650 (1990).
28. Z. Shi, R. J. Boyd, *J. Am. Chem. Soc.* **112**, 6789 (1990).
29. J. M. Riveros, M. Sena, G. H. Guedes, L. A. Xavier, R. Slepetys, *Pure Appl. Chem.* **70**, 1969 (1998).
30. J. M. Gonzales, R. S. Cox III, S. T. Brown, W. D. Allen, H. F. Schaefer III, *J. Phys. Chem. A* **105**, 11327 (2001).
31. The ab initio calculations were performed with the Gaussian computer program package [M. J. Frisch *et al.*, Gaussian98 (Gaussian, Pittsburgh, PA, 1998)].
32. J. W. Larson, T. B. McMahon, *J. Am. Chem. Soc.* **105**, 2944 (1983).
33. K. Fukui, *J. Phys. Chem.* **74**, 4161 (1970).
34. W. L. Hase *et al.*, *Quantum Chem. Program Exch.* **16**, 671 (1996).
35. G. H. Peslherbe, H. Wang, W. L. Hase, in *Advances in Chemical Physics*, vol. 105, D. M. Ferguson, J. I. Siepman, D. G. Truhlar, Eds. (Wiley, New York, 1999), pp. 171–201.
36. J. M. Millam, V. Bakken, W. Chen, W. L. Hase, H. B. Schlegel, *J. Chem. Phys.* **111**, 3800 (1999).
37. V. Bakken, J. M. Millam, H. B. Schlegel, *J. Chem. Phys.* **111**, 8773 (1999).
38. W. L. Hase, D. G. Buckowski, K. N. Swamy, *J. Phys. Chem.* **87**, 2754 (1983).
39. W. L. Hase, *Chem. Phys. Lett.* **67**, 263 (1979).
40. The PST model used here assumes a loose TS with properties identical to those of the reaction products [C. E. Klots, D. Mintz, T. Baer, *J. Chem. Phys.* **66**, 5100 (1977)].
41. X. Hu, W. L. Hase, *J. Phys. Chem.* **96**, 7535 (1992).
42. G. H. Peslherbe, W. L. Hase, *J. Chem. Phys.* **105**, 7432 (1996).
43. R. G. Woolley, *Adv. Phys.* **25**, 27 (1976).

44. Financial support for this research was generously provided by NSF.

14 November 2001; accepted 19 March 2002